A Mathematical Model of the Ocean Boundary Layer under Drifting Melting Ice

U. SVENSSON

Computer-aided Fluid Engineering, Krokvägen 5, Norrköping, Sweden

A. OMSTEDT

Swedish Meteorological and Hydrological Institute, Norrköping, Sweden

(Manuscript received 13 June 1988, in final form 4 April 1989)

ABSTRACT

A mathematical model of the ocean boundary layer under drifting melting ice is formulated, verified, and applied. The model is based on the conservation equations for heat, salt, and momentum and uses turbulence models to achieve closure. Novel features of the model include a low-Reynolds number turbulence model for the viscous region and a discrete element approach to the parameterization of roughness.

Basic verification studies, using laboratory measurements, include the budget of turbulent kinetic energy and the mean temperature profile. All verification studies are focused on the viscous region. Good agreement with measurements is generally obtained.

The model is finally compared to field data obtained during MIZEX. Predicted melt rates are in good agreement with measurements. An analysis of the fluxes of salt and heat within the boundary layer is also provided.

1. Introduction

It is interesting, as a historical note, that our present mathematical description of geophysical boundary layers originates from ice drift studies in the beginning of this century (Ekman 1905). One may further claim that the paper by McPhee and Smith (1976) provided the first simultaneously measured mean current and turbulent stress profiles in an ocean boundary layer. These measurements were obtained from a drifting ice floe. It may well prove to be the case that the recent experimental programs dealing with the marginal ice zone, MIZEX (*J. Geophys. Res.*, Vol. 88, No. C 5, 1983, and Vol. 92, No. C 7, 1987) will have a similar impact on our understanding of geophysical boundary layers. The detailed information provided has already challenged mathematical modellers to simulate, for example, melt rates (McPhee et al. 1987). The present paper, which attempts to simulate the entire boundary layer under drifting ice, also rests on the results from MIZEX.

The boundary layer under drifting ice is schematically shown in Fig. 1. A prominent feature of this boundary layer is the large roughness elements, which are due to ridged ice. McPhee (1986) has compared the ice keels, which are typically 1–5 m in depth, to topographic features in the atmospheric boundary layer. He found, by a scale argument, that they correspond to hills of 30–150 m height. One may therefore expect that ice keels behave more like roughness elements *within* the ocean boundary layer and should not be considered as surface roughness. In the present paper we will use a "discrete element approach," based on the form drag excited by the elements on the water (Taylor et al. 1985). The increased drag due to ice keels will thus not be parameterized as a boundary condition, but appear as source terms in the momentum equations. A similar approach has recently been used in boundary-layer meteorology when studying air flow in and above a forest canopy (Yamada 1982; Raupach and Thom 1981). In Fig. 1 it is indicated that we will idealize the ice keels as conical elements with a circular cross section, a bottom diameter equal to D_r, a depth h_r, and an average spacing Δ_r. Recent field observations (see Wadhams 1988), support the conical sparsely distributed roughness elements indicated in Fig. 1.

The melt rate is, of course, basically controlled by the heat flux to the ice–water interface. The process is, however, quite intricate, as the freezing (or melting) temperature is a function of the salinity at the interface. The salinity at the interface is, in turn, affected by the melt rate, as the melting ice has a much lower salinity. To our understanding it is not suitable to use wall-functions in a situation like this, as additional assumptions about the interface salinity then need to be introduced. Instead we choose to use a model that can be applied all the way into the ice–water interface. By resolving the viscous layer it is expected that the afore-

Corresponding author address: Dr. Anders Omstedt, Swedish Meteorological and Hydrological Institute, S-601 76 Noorköping, Sweden.

© 1990 American Meteorological Society

Unauthenticated | Downloaded 02/05/23 06:52 AM UTC

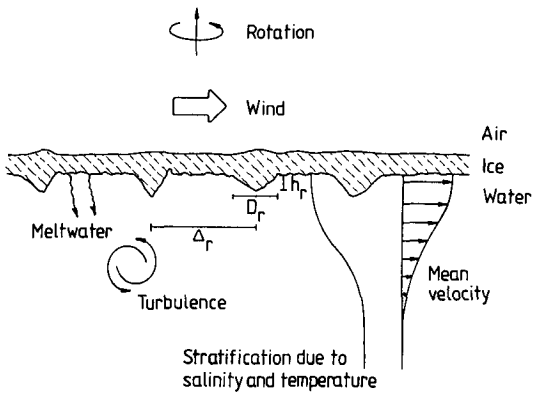

FIG. 1. Schematic figure of the ocean boundary layer under drifting melting ice.

mentioned problem with wall-functions can be avoided, as both temperature and salinity are calculated from their conservation laws right into the ice–water interface. In this context it is relevant to mention that McPhee et al. (1987) have tried different wall-function formulations. The conclusion was that the fully turbulent models, based on a logarithmic profile assumption, overestimates melting while viscous sublayer models predict melt rates too low. Also the uncertainty introduced by roughness was brought up by McPhee et al. A further argument for resolving the viscous sublayer can be found in the discussions of buoyancy effects due to the meltwater (Josberger 1983, 1984; McPhee 1984). In a turbulence closure model it is possible to include buoyancy effects and thus explicitly take this effect into account.

The mathematical model outlined thus attempts to resolve a boundary layer that includes the viscous region, the buffer layer, the logarithmic layer, the Ekman layer, and the geostrophic region. This approach to modeling of the boundary layer under drifting ice, i.e. explicit resolution of roughness elements and viscous region, has to the authors' knowledge not been considered by the recently published papers on modeling (Lemke and Manley 1984; Ikeda 1986; Mellor et al. 1986; McPhee et al. 1987; Häkkinen 1987; Lemke 1987).

The purpose of the present paper is thus to formulate and explore a mathematical model of the ocean boundary layer under drifting melting ice. The low Reynolds number turbulence model will be verified against laboratory measurements, and the complete model will then be applied to situations typical for MIZEX.

2. Mathematical model

The mathematical model to be derived is based on the conservation laws for mass, energy and momentum in their differential form. Models of this kind require turbulent exchange coefficients, which in the present model are calculated from a turbulence model. It will be assumed that the boundary layer is horizontally homogeneous, which implies that the model is one dimensional. With the introduction of the Coriolis term, we thus have arrived at a model describing the idealized planetary boundary layer, which is a suitable frame work for the present problem.

The natural upper boundary of the model is the melting ice–seawater interface. This means, however, that the computational grid will be moving with a velocity equal to the melt velocity. Although this velocity is very small indeed, it will be included in the mathematical formulation, as it may prove important to consider the advective transport of salt in the viscous region of the boundary layer.

a. Mean flow equations

With the assumptions introduced, the momentum equations read

$$\frac{\partial U}{\partial t} + W\frac{\partial U}{\partial z} = \frac{\partial}{\partial z}\left((\nu + \nu_T)\frac{\partial U}{\partial z}\right) + F_U + fV \quad (1)$$

$$\frac{\partial V}{\partial t} + W\frac{\partial V}{\partial z} = \frac{\partial}{\partial z}\left((\nu + \nu_T)\frac{\partial V}{\partial z}\right) + F_V - fU \quad (2)$$

where U and V are horizontal velocities, W is vertical velocity, z is vertical space coordinate (positive upwards), t is time, $\nu\ (=10^{-6}\ \mathrm{m^2\ s^{-1}})$ and ν_T are laminar and turbulent kinematic viscosity, f is Coriolis parameter and F_U and F_V are form drag terms.

The form drag terms represent the influence of the roughness elements. The basic idea behind this approach to roughness parameterization is simply that an object immersed in a flow will exert a force on the fluid. For the present formulation it is probably the only possible approach, considering that the viscous sublayer of thickness, of the order 10^{-3} m, is to be resolved together with roughness elements with a height of 1–10 m. The blockage effect of the elements will not be considered in the present formulation, which assumes that the elements are sparsely distributed. This assumption is also implied when neglecting heat and mass exchange with the roughness elements and in the parameterization of the drag force, as the element density does not appear in the formulae for the drag coefficient. This roughness model, the discrete element approach (Taylor et al. 1985), allows a detailed description of the geometry of the roughness elements (height, spacing, etc.) but, of course, requires that this information is available. In the present paper it will be assumed that all roughness elements are identical and have the shape of a cone. The form drag terms are given by

$$F_U = \frac{1}{2} C_d A_p |U_{\mathrm{ice}} - U|(U_{\mathrm{ice}} - U) \quad (3)$$

$$F_V = \frac{1}{2} C_d A_p |V_{\mathrm{ice}} - V|(V_{\mathrm{ice}} - V) \quad (4)$$

Unauthenticated | Downloaded 02/05/23 06:52 AM UTC

where U_{ice} and V_{ice} are the velocity components for the ice, A_p is the projected area of the roughness elements in the flow direction per unit volume and C_d is an empirical drag coefficient. It is simple to show that A_p is related to Δ_r and $d_r(z)$ by $A_p = d_r(z)/\Delta_r^2$, where $d_r(z)$ is the diameter of the element at level z. For elements with a cross section, which can be approximated as circular, C_d is fairly well represented as a function of a roughness element Reynolds number $\mathrm{Re}_D = [(U_{ice} - U)^2 + (V_{ice} - V)^2]^{1/2} d_r(z)/\nu$. Following Taylor et al. (1985), C_d is given by

$$\log C_d = -0.125 \log(\mathrm{Re}_D) + 0.375, \quad \mathrm{Re}_D < 6 \times 10^4 \tag{5}$$

$$C_d = 0.6, \quad \mathrm{Re}_D \geq 6 \times 10^4. \tag{6}$$

Further details and verification studies of the discrete element approach can be found in Taylor et al. (1985).

The equations for temperature and salinity are

$$\frac{\partial T}{\partial t} + W\frac{\partial T}{\partial z} = \frac{\partial}{\partial z}\left[\left(\frac{\nu}{\mathrm{Pr}_L} + \frac{\nu_T}{\mathrm{Pr}_T}\right)\frac{\partial T}{\partial z}\right] \tag{7}$$

$$\frac{\partial S}{\partial t} + W\frac{\partial S}{\partial z} = \frac{\partial}{\partial z}\left[\left(\frac{\nu}{\mathrm{Sc}_L} + \frac{\nu_T}{\mathrm{Sc}_T}\right)\frac{\partial S}{\partial z}\right] \tag{8}$$

where Pr_L (=13.8), Sc_L (=2432) and Pr_T (=0.86), Sc_T (=0.86) are laminar and turbulent Prandtl and Schmidt numbers. In the present paper, the laminar Prandtl and Schmidt numbers are set to constant values in accordance with McPhee et al. (1987). The value of Pr_T and Sc_T is the generally recommended one for wall boundary layers; see for example Kader and Yaglom (1972). It will be assumed that no exchange of heat or mass with the roughness elements takes place, and hence no source/sink terms are present in (7) and (8).

b. *Turbulence models*

Two turbulence models will be used in the present formulation: a low-Reynolds number model for the near-ice region and a high-Reynolds number model for the outer region. The high-Reynolds number model is the k–ϵ model, which by the present authors, Svensson (1979), Omstedt et al. (1983), has been successfully applied to geophysical boundary layers. A general review of this model is given by Rodi (1987). The model is based on transport equations for the turbulent kinetic energy, k, and its dissipation rate, ϵ. These equations read

$$\frac{\partial k}{\partial t} + W\frac{\partial k}{\partial z} = \frac{\partial}{\partial z}\left(\frac{\nu_T}{\sigma_k}\frac{\partial k}{\partial z}\right) + P_s + P_b - \epsilon \tag{9}$$

$$\frac{\partial \epsilon}{\partial t} + W\frac{\partial \epsilon}{\partial z} = \frac{\partial}{\partial z}\left(\frac{\nu_T}{\sigma_\epsilon}\frac{\partial \epsilon}{\partial z}\right) + \frac{\epsilon}{k}\left[C_{1\epsilon}P_s + C_{3\epsilon}P_b - C_{2\epsilon}\epsilon\right] \tag{10}$$

$$P_s = \nu_T\left[\left(\frac{\partial U}{\partial z}\right)^2 + \left(\frac{\partial V}{\partial z}\right)^2\right] \tag{11}$$

$$P_b = \nu_T g\left[-2\alpha_1\frac{T - T_M}{\mathrm{Pr}_T}\frac{\partial T}{\partial z} + \frac{\alpha_2}{\mathrm{Sc}_T}\frac{\partial S}{\partial z}\right] \tag{12}$$

where P_s denotes shear production and P_b buoyancy production. The kinematic eddy viscosity is calculated from the Prandtl–Kolmogorov expression:

$$\nu_T = C_\mu k^2/\epsilon. \tag{13}$$

The reader is referred to the papers for details of this model.

A one-equation turbulence model will be used in the region close to the ice–seawater interface. This region will cover the viscous layer and the roughness elements, and the coupling to the two-equation model is thus made outside the roughness elements. There are two reasons for using a one-equation model in the near-ice region. First, our verification studies (this paper and Svensson and Rahm 1988) of this model have shown that the one-equation model is as good as, or superior to, the low-Reynolds number versions of the k–ϵ model. Second, the roughness elements modifies the ϵ-equation in an unknown way. However, for the one-equation model, where the length scale is to be prescribed, a tentative relation that takes roughness elements into account is available. The drawback of using two turbulence models is that one needs to specify a point where to switch from one model to the other. Generally speaking, one chooses a point which gives a smooth transition (in terms of k and ν_T) from one model to the other. In the present study this point was set at a distance of $1.2h_r$, where h_r is the height of the roughness elements, from the ice water interface. The one-equation model is based on an equation for k and a prescribed length scale. Viscous effects are taken into account in the k-equation and the Prandtl–Kolmogorov expression. The equations read:

$$\frac{\partial k}{\partial t} = \underbrace{\frac{\partial}{\partial z}\left[\left(\nu + \frac{\nu_T}{\sigma_k}\right)\frac{\partial k}{\partial z}\right]}_{\text{Diffusion}} + \underbrace{P}_{\text{Production}} \underbrace{- \frac{2\nu k C_D}{l^2} - \frac{C_D k^{3/2}}{l}}_{\text{Dissipation}} f_\mu \tag{14}$$

$$\nu_T = C'_\mu k^{1/2} l f_\mu \tag{15}$$

$$P = \underbrace{\nu_T\left(\frac{\partial U_l}{\partial z}\right)^2}_{\text{Shear}} + \underbrace{P_b}_{\text{Buoyancy}} \underbrace{+ \frac{1}{2} C_d A_p U_l^2 |U_l|}_{\text{Form drag}} \tag{16}$$

$$f_\mu = 1 - \exp(-A_\mu R_k) \tag{17}$$

$$R_k = k^{1/2} l/\nu \tag{18}$$

Unauthenticated | Downloaded 02/05/23 06:52 AM UTC

where R_k is a turbulence Reynolds number, f_μ is a damping function, l is the prescribed length scale, C_D (=0.164), C'_μ (=0.5477) and A_μ (=0.03) are empirical constants. Since the one-equation model is to be used only close to the ice, only one horizontal velocity component, denoted U_l, is included in the formulation. This velocity has, of course, two components in the basic coordinate system. The important low-Reynolds number features of this model are due to the dissipation term in Eq. (14) and the damping function f_μ. Of the two dissipation terms, the first one is dominant for low R_k, as can be understood by noting that it is proportional to ν. The second part is the standard dissipation term in one-equation models for high Reynolds numbers, except for f_μ. This function goes to 1.0 for high R_k and to zero for low R_k, and thus it makes the second dissipation term Reynolds number-dependent. The formulation and the constants of this model are given by Spalding and Elhadidy (1979), who also carried out detailed verification studies. It should be noted, however, that they only considered smooth boundaries, and thus the third production term in expression (16) was not present. One may therefore question the validity of the empirical constants which were established for smooth conditions. In between the sparsely distributed roughness elements, however, we do assume a smooth boundary, and the influence of the roughness elements is therefore through the friction velocity, which is the scaling velocity for the viscous sublayer. We may therefore, alternatively, classify the model as a model for smooth ice with a friction velocity modified by roughness elements. Another reason for keeping the original constants is that the model should approach the smooth boundary version when the typical distance between the roughness elements goes to infinity. Similar formulations are also discussed by Reynolds (1976). A recent application of this model to the flow and heat transfer over a circular cylinder is reported by Ibrahim (1987). Another recent application (Svensson and Rahm 1988) deals with the near-bottom region of the benthic boundary layer. It is beyond our present scope to describe this model in more detail; instead the reader is referred to the papers mentioned and the papers by Patel et al. (1985) and Nagano and Hishida (1987), where low-Reynolds number models in general are discussed and evaluated.

The specification of length scale is simple in the absence of roughness elements; it may for the wall-region be set as κz, where κ is the von Kármán constant. The roughness elements do, however, modify the length-scale in an unknown way. A tentative modification of the length-scale specification is derived and tested in Svensson and Rahm (1988). This specification reads:

$$l = -\hat{l} + [\hat{l}^2 + (\kappa z)^2]^{1/2} \tag{19}$$

$$\hat{l} = \frac{C_d A_p |U_l|^3}{2C'_\mu k^{1/2} (\partial U_l/\partial z)^2}. \tag{20}$$

This formulation is seen to return to κz in the absence of roughness elements. Details of the application of this length-scale equation can be found in Svensson and Rahm (1988).

c. Equation of state

Stratification is in the present formulation due to salinity and temperature gradients. A nonlinear density–temperature dependence is assumed, while the density is linearly related to salinity:

$$\rho = \rho_0[1 - \alpha_1(T - T_M)^2 + \alpha_2 S] \tag{21}$$

where α_1 (=7×10^{-6}) and α_2 (=8×10^{-4}) are expansion coefficients and T_M the temperature of maximum density. The T_M is a function of salinity and pressure (see Caldwell 1978) but will in the present study be assumed constant and equal to −2.7°C. The equation of state could probably be simplified further for the calculations described in the present paper, but Eq. (21) is used with future applications in mind.

d. Boundary conditions

For the momentum equations, the upper boundary condition is a specified velocity—the ice drift velocity. At the lower boundary, a zero stress condition is used, equivalent to a zero velocity gradient condition.

Temperature and salinity are specified at the lower boundary to values given by measurements. These values thus give the mixed layer properties. At the ice–seawater interface, the boundary condition for salinity is that of a given flux. The flux is given by the melt rate and the salinity of the ice, S_{ice}:

$$\text{flux}_s = \frac{dh}{dt} S_{\text{ice}} \tag{22}$$

where dh/dt is the melt rate. This simple boundary condition applies due to the moving grid adopted and because the viscous sublayer is resolved. If, for example, the ice salinity is zero, a zero flux will result. The salinity at the interface, if diffusion is neglected, will then decrease because salt is transported out of the cell by advection, see Eq. (8). The advection velocity is equal to the melt rate. If a steady state is reached, a balance between advection (from the boundary) and diffusion (towards the boundary) is established. This balance will be analyzed in detail below. The temperature at the ice–seawater interface is specified as the freezing temperature for the salinity at the interface, S_0. The dependence on pressure in this relation (see Millero, 1978) is neglected for the present situation. The relation used reads:

$$T_f = -0.0575 S_0 + 1.710523 \times 10^{-3} S_0^{3/2} - 2.154996 \times 10^{-4} S_0^2. \tag{23}$$

With a specified temperature at the interface, a heat flux can be obtained from Fouriers law, i.e.:

Unauthenticated | Downloaded 02/05/23 06:52 AM UTC

$$\text{flux}_h = \frac{\nu}{\text{Pr}_l} \frac{\partial}{\partial z} \rho C_p T \tag{24}$$

where C_p is the specific heat of seawater. The specific heat of seawater is a function of temperature, salinity, and pressure (Gill 1982) but is here set to a constant value equal to 3980 J (kg °C)$^{-1}$. The temperature gradient is evaluated from T_f and the temperature of the cell closest to the ice–water interface. Strictly, advective heat transport should enter this flux, but it can be shown by estimating the Peclet number that the advective transport is two orders of magnitude smaller than the conduction contribution. This heat flux gives the melt rate through the expression:

$$\frac{dh}{dt} = \text{flux}_h / L\rho_{\text{ice}} \tag{25}$$

where L is the latent heat of saline ice. As the melt rate also determines the grid movement, it is clear that $dh/dt = W$, where W is the vertical velocity appearing in the conservation equations above.

As can be seen, simple boundary conditions for temperature and salinity apply in the present formulation. In fact, one of the major advantages of the moving grid and the resolution of the viscous sublayer is that straightforward boundary conditions apply. Boundary conditions for turbulent kinetic energy and its dissipation rate are also straightforward in the present formulation. At the lower boundary zero gradient conditions are used, while at the upper boundary, where the one-equation model is used, k is specified to zero.

e. *Numerical solution*

The set of equations formulated are solved using the equation solver PROBE (Svensson 1986). PROBE is a finite-difference code based on an implicit numerical scheme. The vertical extent of the grid cells was increased down from the ice–water interface, with a typical number of cells equal to 70. The cell closest to the ice was typically 2×10^{-5} m. This extremely small cell size is motivated by the correspondingly thin diffusion layer for salt. For the present conditions it can be shown that this layer has a thickness of the order 10^{-4} m. Predictions to be presented in the next section were tested for grid-independence, and the predictions can therefore be regarded as an accurate solution of the differential equations.

3. Results of calculations

Basic verification studies of the low-Reynolds number turbulence model and the discrete element approach to roughness are presented in Svensson and Rahm (1988). As the present paper focuses attention on the processes at the ice–seawater interface, some additional verification studies of the turbulence energy budget in the low-Reynolds number region will be presented in the present paper. We will then apply the model to a situation with conditions close to day 191 during the MIZEX experiment (McPhee et al. 1987). Details of the boundary layer structure, as predicted by the model, are provided. Finally, a transient situation, covering the days 188–192 during MIZEX, is considered.

a. *The low-Reynolds number region*

This verification study makes use of some recently presented data on the near-wall region of a boundary layer. The surface is hydrodynamically smooth, and no buoyancy effects are present. Measurements of the turbulent kinetic energy budget have been carried out by Johansson and Karlsson (1988). These data are presented in Fig. 2 together with results from the present low-Reynolds-number turbulence model. As can be seen, a close agreement exists. The experimental data by Johansson and Karlsson were obtained from Laser Doppler Velocity measurements. The budget was obtained by measuring shear production, viscous diffusion, and turbulent diffusion. Pressure diffusion was neglected, as it is believed to be a higher order term, and dissipation was obtained as the closing term. It is interesting to note that the direct simulation results by Spalart (1988) are in close agreement with the budget shown in Fig. 2.

A comparison with the mean velocity profile measured by Johansson and Karlsson (1988) is also shown in Fig. 2. Once again the agreement is very satisfactory.

As the melt rate is controlled by the heat transfer to the ice–water interface, it is of interest to include a temperature profile in the verification study. The laboratory measurements of Antonia et al. (1977) are used for this purpose. A laminar Prandtl number of 0.72 was used in this simulation, as the measurements were carried out in a wind tunnel. The comparison between the nondimensional profiles is shown in Fig. 3. The agreement is also regarded as satisfactory for this case.

In the near-ice region of the ocean boundary layer, additional complicating features like roughness, melting, density variations, etc. are found. The method of verification in the present model development has, however, been to verify different aspects of the model by comparisons with available laboratory experiments. It has thus been demonstrated that the mean velocity profile, k-budget and temperature profile are accurately predicted through the viscous sublayer. The roughness model adopted was, as mentioned above, verified in Svensson and Rahm (1988). The combined effect of, for example, melting and roughness is not verified by this approach, and the verification study is therefore not conclusive.

b. *Day 191, 1984, in MIZEX*

McPhee et al. (1987) analyzed day 191 of MIZEX and also applied different theoretical models. The basic

Unauthenticated | Downloaded 02/05/23 06:52 AM UTC

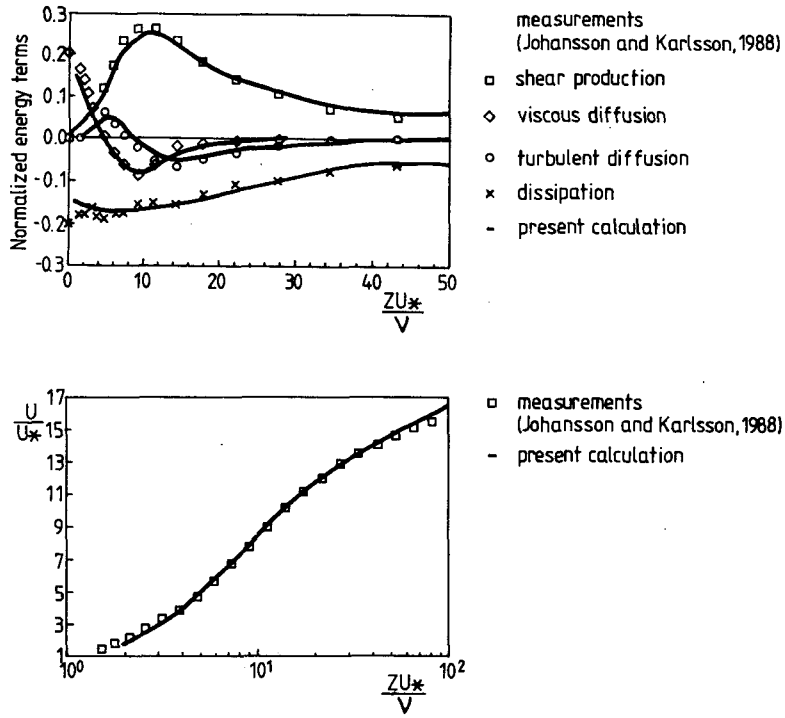

FIG. 2. Turbulent kinetic energy budget (top) and mean velocity profile (bottom). The terms in the energy budget are normalized with ν/U_*^4.

average properties of the boundary layer for this day were given by McPhee et al. (1987). If the mixed layer temperature and salinity are fixed, a steady state solution can be obtained, which is useful for a detailed analysis of the boundary layer. The steady state, it should be pointed out, is in the moving coordinate system. A constant advection velocity is thus balanced by molecular and turbulent diffusion of salt and heat. The following data were used for the calculations to be presented: $U_{ice} = 0.25$ m s^{-1}, $T_\infty = -0.3$°C, $S_\infty = 33$‰, $S_{ice} = 4$‰, $D_r = 1.0$ m and $h_r = 2.0$ m. The lower boundary was set at 28.0 m below the ice–water interface. The roughness height chosen, h_r, is based on the estimates $z_0 = 0.066$ m and $h_r = 30z_0$ given by McPhee et al. (1987). In the form drag terms (3) and (4) it is the projected area per unit volume, A_p, of the roughness elements that enters, which indicates that one may fix the diameter, D_r, and vary the spacing, Δ_r, in order to cover a range of A_p. A weak depenence of D_r is, however, present through the C_d coefficient. We choose to fix D_r to 1.0 m and vary the spacing in order to see the influence of roughness.

Results of predictions are shown in Fig. 4. Melt rate, interface salinity, and heat transfer coefficient are shown as a function of the spacing between the roughness elements. The calculations are seen to be in general agreement with the field measurements by Josberger (1987) for the heat transfer coefficient and also with the melt rate estimated by McPhee et al. (1987) for day 191. It is also interesting to note that assuming a hydrodynamically smooth surface ($\Delta_r = \infty$) also gives a melt rate of the correct order of magnitude. An assumption introduced above is that heat and mass exchange with the roughness elements can be neglected. A reasonable requirement is then that the surface area of the roughness elements should be at least an order of magnitude smaller than the smooth ice boundary. For the present conditions this means that $\Delta_r > 5.0$ m, which indicates that predictions for $\Delta_r < 5.0$ m become

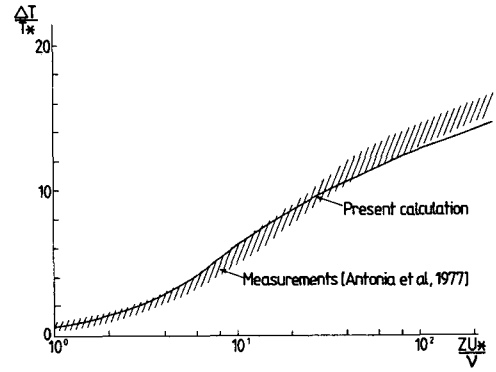

FIG. 3. Comparison of predicted temperature profile with measurements of Antonia et al. (1977). The temperature has been normalized with $T_* (=Q/\rho C_p U_*)$.

Unauthenticated | Downloaded 02/05/23 06:52 AM UTC

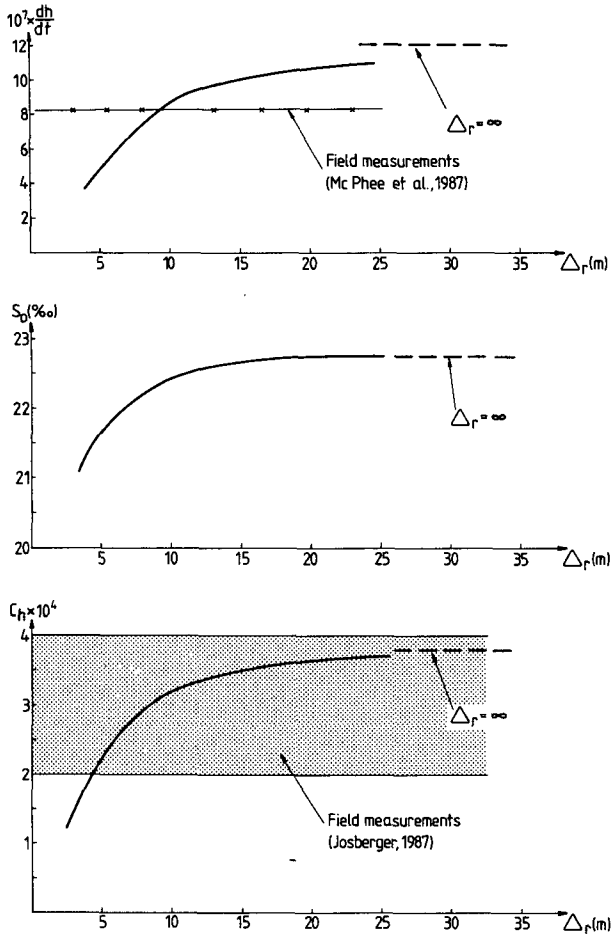

FIG. 4. Comparison of predicted melt rate (top), interface salinity (middle) and heat transfer coefficients (bottom) with field measurements from MIZEX 1984.

increasingly unrealistic. Vertical profiles of velocity, temperature, and salinity are given in Fig. 5 for $\Delta_r = 10$ m. In Fig. 5 one should note that the velocity profile is logarithmic in the turbulent part of the flow (as it is almost linear in the log-scale used). We may further note that the salinity change over the boundary layer occurs very close to the ice, $O(10^{-3}$ m). This is, of course, due to the high molecular Schmidt number for salt, as can be understood from a comparison with the temperature profile.

A detailed analysis of the terms in the salinity equation can be found in Fig. 6. Looking first at the magnitude of the terms in the differential equation, Fig. 6a, one finds that terms of large magnitude are found only very close to the ice. The explanation can be found in Fig. 6b, where salt fluxes are shown. First, one need to remember that the coordinate system is attached to the melting ice–seawater interface. This means that in the steady state situation considered, a net flux towards the mixed layer, proportional to the salinity in the melting ice, must be present. However, diffusion, molecular and turbulent, will always transport salt towards the interface, as this is in the direction of the negative gradient. Hence the advection must everywhere be larger than the sum of molecular and turbulent diffusion with an amount equal to the constant net flux given by the melting ice. If we next consider the shape of the curve describing the advective transport, one should first note that the volume flux is constant and equal to the melt rate, through the entire boundary layer. The decrease of the curve towards the ice is thus due to the decrease in salinity. By once again requiring a constant net flux, we also understand the shape of the molecular diffusion curve as it approaches the ice. Figure 6b is seen to reproduce exactly this picture. Returning now to Fig. 6a, one should note that the terms in the differential equation describe the gradient of fluxes. Looking at molecular diffusion, for example, it is clear that the gradient of the flux changes sign, and accordingly the differential term changes sign. It is also clear that all flux gradients are small in the turbulent part of the boundary layer.

The same analysis for heat is presented in Figs. 7a and 7b. Looking first at the fluxes, one notes that the net flux is in the direction of decreasing temperature. The direction of the net heat flux is upwards, as the ice is melting. Molecular and turbulent diffusion are the dominating modes of transport, advection is two orders of magnitude smaller than the net flux. The smaller influence of advection is also seen in Fig. 7a.

The detailed analysis presented of the boundary layer under melting, drifting ice illustrates the complexity of the problem. Even with all the simplifying assumptions introduced, it is hard to understand all fluxes and balances present. The mathematical model presented, however, does give a consistent and detailed picture of the physical processes involved.

c. Days 188–192, 1984, during MIZEX

Mixed layer temperature and salinity and ice drift velocity were measured continuously during MIZEX. McPhee et al. (1987) provide data for the days 188–192, during which the mixed layer properties varied significantly. In Fig. 8 the measured ice drift and the idealization made for the numerical model calculations are shown. As seen, we neglect the variation in direction during the drift. The spacing between roughness elements was also for this case assumed to be 10 m. Initial conditoins (day 188) for salinity and temperature were set as uniform profiles of 33‰ and −1.5°C. At the end of day 190 a front passed, which brought new water into the boundary layer. In the numerical model this front was simulated by simply prescribing new values to salinity (=33.1‰) and temperature (−0.5°C) at the end of day 190. These data were evaluated from McPhee et al. (1987). Measured and predicted melt rates are shown in Fig. 8. Qualitatively the agreement is satisfactory, although the measurements show a more

Unauthenticated | Downloaded 02/05/23 06:52 AM UTC

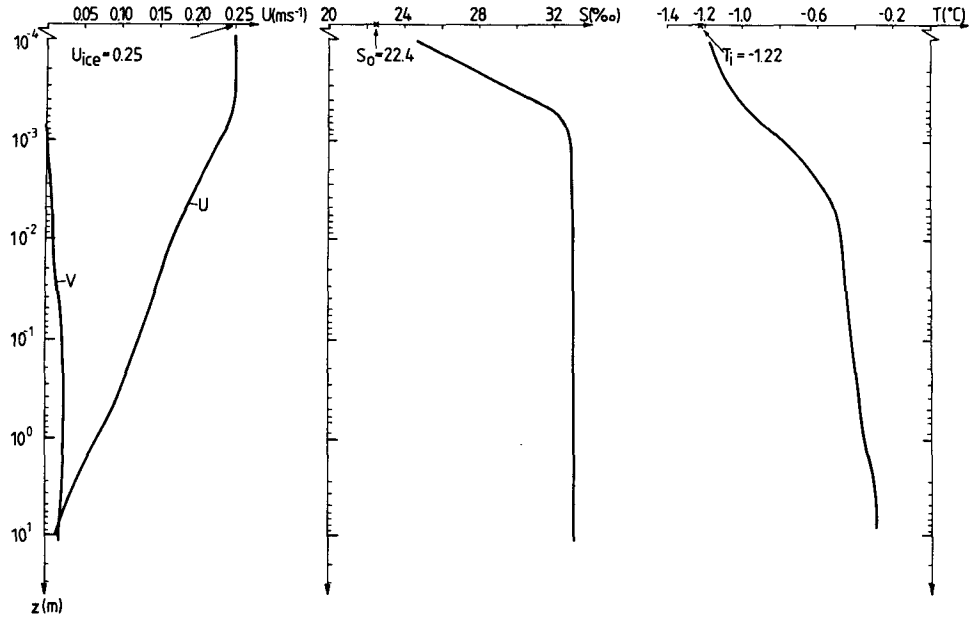

FIG. 5. Predicted velocity, salinity and temperature profiles for day 191 of MIZEX 1984.

gradual response to the change in the mixed layer properties. This may be partly due to the idealized forcing in the numerical model, but it probably also shows the limitations of a one-dimensional analysis.

4. Discussion and conclusions

A mathematical model of the boundary layer under drifting melting ice is bound to have "weak spots" considering the complexity of the problem. In the model presented we believe that it is the treatment of roughness elements that introduces one of the main uncertainties. The approach is probably sound, but the modification of the turbulence model constitutes a major problem. In the present work, following Svensson and Rahm (1988), the length-scale distribution is modified in the presence of roughness. The tentative relations used, although to some degree tested by Svensson and Rahm (1988), certainly need further

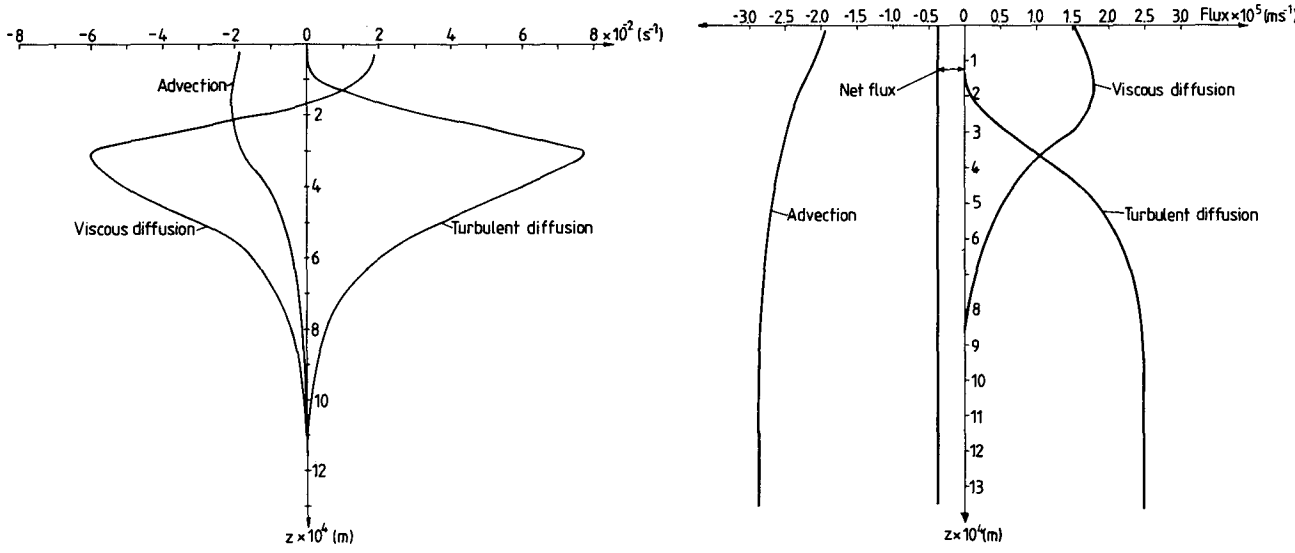

FIG. 6. The salt balance of the boundary layer for day 191 of MIZEX 1984. Terms in the differential equation (a: left panel) and fluxes (b: right panel) as given by the mathematical model.

Unauthenticated | Downloaded 02/05/23 06:52 AM UTC

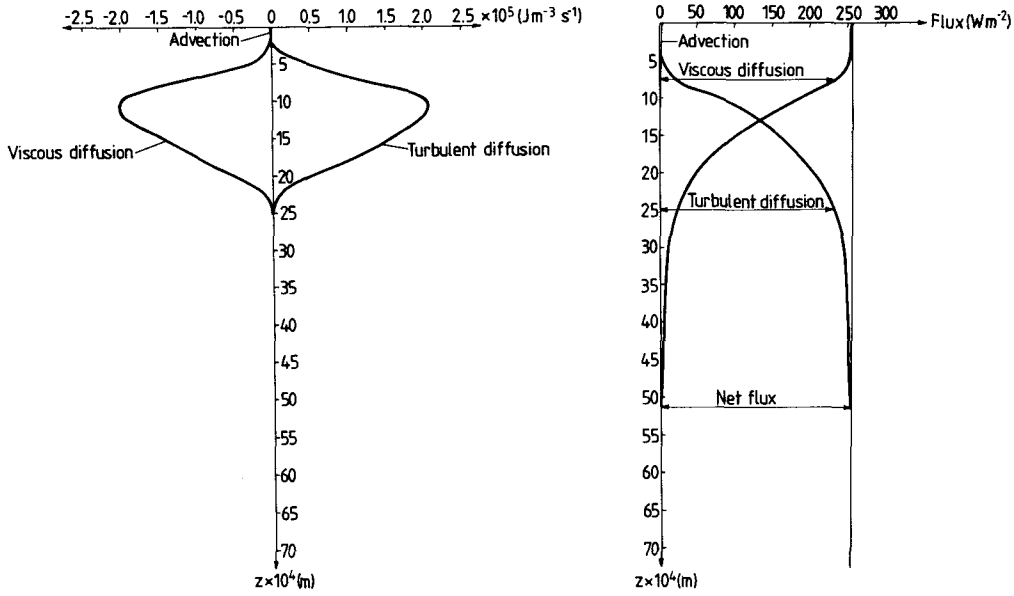

FIG. 7. The heat balance of the boundary layer for day 191 of MIZEX 1984. Terms in the differential equation (a: left panel) and fluxes (b: right panel) as given by the mathematical model.

consideration. The low-Reynolds-number model used seems to be in close agreement with available experimental data. It is, however, instructive to note that the turbulent transport of salt is as effective as the molecular transport when the ratio ν_T/ν is of the order 10^{-3}. This can be understood by writing the total diffusive transport coefficient as $(\nu/\mathrm{Sc}_L + \nu_T/\mathrm{Sc}_T)$ and noting that the Sc_L is about three orders of magnitude larger than Sc_T. It is questionable if one can trust predicted eddy viscosities of this magnitude.

The close agreement with laboratory and field data obtained with the model presented does indicate, however, that the formulation is basically sound. It is noteworthy that no constants in the model have been tuned for the present application. We may thus consider the formulation as a theoretical frame work, which contains submodels that need to be refined and further tested.

The conclusions from the paper may be summarized as:

- A mathematical model of the ocean boundary layer under drifting, melting ice can, and has been, formulated. The model contains submodels for low- and high-Reynolds number turbulence and also for distributed roughness elements.
- The low-Reynolds number turbulence model is found to predict a turbulence energy budget in the near-wall region of a boundary that is in close agreement with measurements. Also the predicted temperature profile through the viscous region is found to be in agreement with laboratory measurements.
- Applications to MIZEX data show satisfactory agreement with measurements. An analysis of the heat and salt fluxes within the boundary layer provides a detailed and consistent picture of the processes taking place under melting, drifting ice.

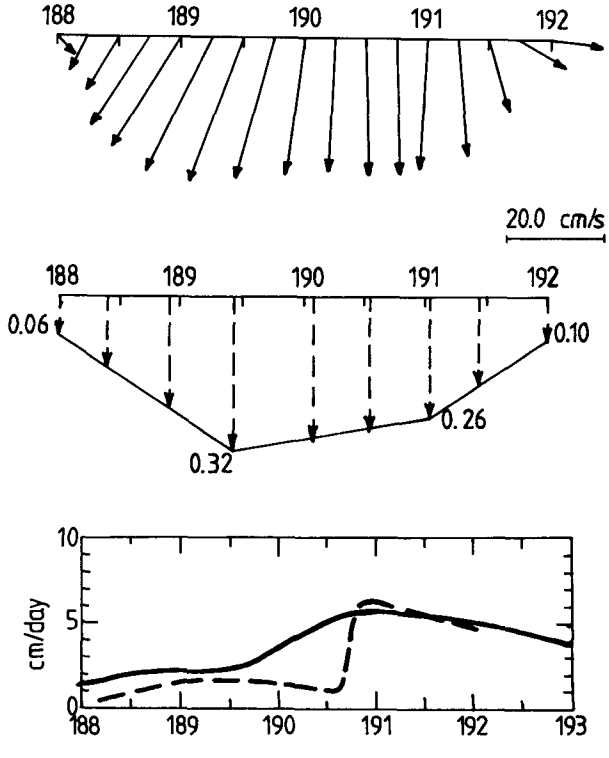

FIG. 8. Comparison (bottom) of measured and predicted melt rate for the days 188–192 of MIZEX 1984. Measured (top) ice drift and idealization (middle) used for numerical simulation are also shown.

Unauthenticated | Downloaded 02/05/23 06:52 AM UTC

Acknowledgments. This work has been financed by the Swedish Administration of Shipping and Navigation and the Swedish Natural Science Research Council.

APPENDIX

List of Symbols

A_p	projected area per unit volume
A_μ	constant in damping function
C_d	drag coefficient
C_μ, C_{1_ϵ}–C_{3_ϵ}	constants in the k–ϵ model
C'_μ, C_D	constant in the one-equation turbulence model
C_p	specific heat of sea water
D_r	roughness element bottom diameter
$d_r(z)$	roughness element diameter
f	Coriolis' parameter
flux_h	heat flux at ice–water interface
flux_s	salinity flux
F_U	form drag in x-direction
F_V	form drag in y-direction
f_μ	damping function
g	gravity constant
h_r	ice keel depth
k	turbulent kinetic energy
L	latent heat of ice
$l, \hat{l}$	length scales
dh/dt	melting rate
P	turbulent kinetic energy production
P_b	buoyancy production/destruction
Pr_l	laminar Prandtl number
Pr_T	turbulent Prandtl number
P_s	shear production
Re_D	roughness element Reynolds number
R_k	turbulence Reynolds number
S	mean salinity
Sc_L	laminar Schmidt number
Sc_T	turbulent Schmidt number
S_0	salinity at ice–water interface
S_{ice}	salinity of ice
T	mean temperature
T_f	freezing/melting temperature
T_M	temperature of maximum density
T_∞	temperature at lower boundary
t	time
S_∞	salinity at lower boundary
U	mean velocity in x-direction
U_l	mean local velocity in drift direction
U_{ice}	mean ice velocity in x-direction
V	mean velocity in y-direction
V_{ice}	mean ice velocity in y-direction
W	mean velocity in z-direction
x	horizontal coordinate, positive in east direction
y	horizontal coordinate, positive in north direction
z	vertical coordinate, positive upwards
α_1, α_2	constants in the equation of state
Δ_r	average spacing of ice keels
ϵ	dissipation rate of turbulent kinetic energy
κ	von Kármán constant
ν	molecular kinematic viscosity
ν_T	turbulent kinematic viscosity
ρ_{ice}	ice density
ρ_0	reference density
σ_ϵ	turbulent Schmidt number for ϵ
σ_k	turbulent Schmidt number for k

REFERENCES

Antonia, R. A., H. Q. Danh, and A. Prabhu, 1977: Response of a turbulent boundary layer to a step change in surface heat flux. *J. Fluid Mech.*, **80**(Part 1), 153–177.

Caldwell, D. R., 1978: The maximum density points of pure and saline water. *Deep-Sea Res.*, **25**, 175–181.

Ekman, V. W., 1905: On the influence of the earth's rotation on ocean currents. *Ark. Mat. Astron. Fys.*, **2**(11), 1–53.

Gill, A. E., 1982: *Atmosphere-Ocean Dynamics. Int. Geophys. Ser.*, Vol. 30, Appendix A 3.4.

Häkkinen, S., 1987: A coupled dynamic–thermodynamic model of an ice-ocean system in the marginal ice zone. *J. Geophys. Res.*, **92**(C 9), 9469–9478.

Ibrahim, M. B., 1987: A turbulence model for the heat transfer near stagnation point of a circular cylinder. *Appl. Sci. Res.*, **44**, 287–302.

Ikeda, M., 1986: A mixed layer beneath melting sea ice in the marginal ice zone using a one-dimensional turbulent closure model. *J. Geophys. Res.*, **91**(C 4), 5054–5060.

Johansson, T. G., and R. I. Karlsson, 1988: The energy budget in the near wall region of a turbulent boundary layer. *Fourth Int. Symp. on Appl. of Laser Anemometry to Fluid Mechanics*, Lisbon.

Josberger, E. G., 1983: Sea ice melting in the marginal ice zone. *J. Geophys. Res.*, **88**(C 5), 2841–2844.

——, 1984: Reply. *J. Geophys. Res.*, **89**(C 1), 761–762.

——, 1987: Bottom ablation and heat transfer coefficients from the 1983 marginal ice zone experiments. *J. Geophys. Res.*, **92**(C 7), 7012–7016.

Kader, B. A., and A. M. Yaglom, 1972: Heat and mass transfer laws for fully turbulent wall flows. *Int. J. Heat Mass Transfer*, **15**, 2329–2351.

Lemke, P., 1987: A coupled one-dimensional sea ice-ocean model. *J. Geophys. Res.*, **92**(C 12), 13 164–13 172.

——, and T. O. Manley, 1984: The seasonal variation of the mixed layer and the pycnocline under polar sea ice. *J. Geophys. Res.*, **89**(C 4), 6494–6504.

McPhee, M. G., 1984: Comment on "Sea ice melting in the marginal ice zone" by Edward G. Josberger. *J. Geophys. Res.*, **89**(C 1), 759–760.

——, 1986: The upper ocean. *The Geophysics of Sea Ice.* N. Untersteiner, Ed., NATO ASI Series B: Physics, Vol. 146, 339–394, Plenum Press.

——, and J. D. Smith, 1976: Measurements of the turbulent boundary layer under pack ice. *J. Phys. Oceanogr.*, **6**, 696–711.

——, G. A. Maykut and J. H. Morrison, 1987: Dynamics and thermodynamics of the ice/upper ocean system in the marginal ice zone of the Greenland Sea. *J. Geophys. Res.*, **92**(C 7), 7017–7031.

Mellor, G. L., M. G. McPhee and M. Steele, 1986: Ice–sea water turbulent boundary layer interaction with melting or freezing. *J. Phys. Oceanogr.*, **16**, 1829–1846.

Millero, F. J., 1978: Freezing point of sea water. Eighth Report of the Joint Panel on Oceanographic Tables and Standards.

Unauthenticated | Downloaded 02/05/23 06:52 AM UTC

UNESCO Tech. Pap. Mar. Sci. No. 28, Annex 6, UNESCO, Paris, France.

Nagano, Y., and M. Hishida, 1987: Improved form of the $k-\epsilon$ model for wall turbulent shear flows. *J. Fluid Eng.*, **109,** 156–160.

Omstedt, A., J. Sahlberg and U. Svensson, 1983: Measured and numerically simulated autumn cooling in the Bay of Bothnia. *Tellus,* **35A,** 231–240.

Patel, V. C., W. Rodi and G. Scheuerer, 1985: Turbulence models for near-wall and low-Reynolds number flows: A review. *AIAA Journal,* **23,** 1308–1319.

Raupach, M. R., and A. S. Thom, 1981: Turbulence in and above plant canopies. *Ann. Rev. Fluid Mech.,* **13,** 97–129.

Reynolds, W. C., 1976: Computation of turbulent flows. *Ann. Rev. Fluid Mech.,* **8,** 183–208.

Rodi, W., 1987: Examples of calculation methods for flow and mixing in stratified fluids. *J. Geophys. Res.,* **92**(C 5), 5305–5328.

Spalart, P. S., 1988: Direct simulation of a turbulent boundary layer up to $R_\theta = 1410$. *J. Fluid Mech.,* **187,** 61–98.

Spalding, D. B., and M. A. Elhadidy, 1979: New approach to calculating turbulent flows in the near-wall region. Imperial College of Science and Technology, HTS/79/9, 1–35, London, England.

Svensson, U., 1979: The structure of the turbulent Ekman layer. *Tellus,* **31,** 340–350.

——, 1986: PROBE—An instruction manual. Report Oceanography No. 10, 90 pp, The Swedish Meteorological and Hydrological Institute (SMHI), S-601 76, Norrköping, Sweden.

——, and L. Rahm, 1988: Modeling the near-bottom region of the benthic boundary layer. *J. Geophys. Res.,* **93**(C 6), 6909–6915.

Taylor, R. P., H. W. Coleman and B. K. Hodge, 1985: Prediction of turbulent rough-wall skin friction using a discrete element approach. *J. Fluid Eng.,* **107,** 251–257.

Wadhams, P., 1988: The underside of Arctic sea ice imaged by side scanner sonar. *Nature,* **33**(No. 6169), 161–164.

Yamada, T., 1982: A numerical model study of turbulent air flow in and above a forest canopy. *J. Meteor. Soc. Japan,* **60**(1), 439–453.

Unauthenticated | Downloaded 02/05/23 06:52 AM UTC